Journal of the European Ceramic Society 20 (2000) 2561–2568

Evolution of defect size and strength of porous alumina during sintering

Brian D. Flinn [a], Rajendra K. Bordia [a], André Zimmermann [b,1], Jürgen Rödel [b,*]

[a] *Department of Materials Science and Engineering, University of Washington, Seattle, WA 98195, USA*
[b] *Department of Materials Science, Darmstadt University of Technology, 64287 Darmstadt, Germany*

Received 9 December 1999; received in revised form 8 May 2000; accepted 14 May 2000

Abstract

The evolution of fracture strength with increasing density in ceramics, using alumina as a model system, is discussed in terms of the interplay between a defect serving as stress concentrator, a crack lying in its enhanced stress field and the fracture toughness of the porous ceramic. Introduction of crack-free fracture-causing artificial pores of various sizes allows detailed measurement of their shrinkage with ongoing densification, while fractography describes the location and type of fracture initiation. A fracture mechanics model, describing growth of a semicircular crack emanating from the pore until instability, yields good agreement with experiment. In particular, the result that the radius of the artificial, spherical defect in a size regime between 25 and 120 μm has only a small influence on fracture strength for samples with an average grain size smaller than 1μm, can be explained.

Keywords: Al_2O_3; Crack growth; Mechanical properties; Porosity; Sintering

1. Introduction

In order to increase the strength and reliability of ceramics, it is necessary to understand how strength evolves during fabrication. In this context, fracture strength can be described as arising from an interplay between the size of the largest defect (worst case) and the fracture toughness of the material (average property).[1–3] Simple analytical descriptions result if the largest porous defect is itself viewed as serving as a crack.[1–3] Mechanical descriptions which are most physically accurate view a failure causing defect as a combination of stress concentrator (e.g. a large pore) and sharp crack,[4–7] but require more elaborate numerical treatment.

Thus, in order to gain a better understanding of how processing parameters influence the strength of ceramics it is critical to combine the evolution of the extreme microstructural features (flaws) with average microstructural features. For cases, where fracture initiates around large pores,[8] thermodynamic stability and kinetic evolution during densification must be considered. Thermodynamics dictates that there exists an equilibrium pore size determined by grain size, the surrounding grain configuration and dihedral angle, as well as applied stress, where pores neither shrink nor grow.[9,10] Kinetic limitations, however, might prevail for other conditions. Therefore, shrinkage of large pores has only been observed for hot isostatic pressing of microstructures exhibiting sufficient plastic deformability.[10,11] Shrinkage of isolated pores in dense materials subject to hydrostatic pressure has been modeled by Evans and Hsueh.[12] Without application of an external pressure, shrinkage of large pores had only been determined in one instance, where pores of a starting radius of 50 μm shrank to about 42 μm.[13]

Recent considerations of the fracture toughness of porous ceramics have utilized a correlation between fracture toughness and elastic modulus.[1–3] The dependence of elastic modulus on density has been studied in detail and can be described with either a linear dependence[1,14] or a slightly non-linear function suggested by

* Corresponding author. Fax: +49-6151-16-6314.
E-mail addresses: dh39@hrzpub.tu-darmstadt.de or rodel@ceramics.tu-darmstadt.de (J. Rödel).
[1] Now at Pulvermetallurgisches Laboratorium, Max-Planck-Institut für Metallforschung and Institut für Nichtmetallische Anorganische Materialien, Universität Stuttgart, Stuttgart, 70569 Germany.

0955-2219/00/$ - see front matter
PII: S0955-2219(00)00133-3

Phani and Niyogi.[2,3,15] Both relationships provide acceptable data fits, except for the very early stage of sintering, where neck growth leads to an increase in elastic modulus with little densification.[16]

Prior studies have determined that the *R*-curve in alumina leads to small closure stresses[17] which are ineffective in raising the fracture strength.[6,18] Appropriate values of the crack tip toughness, K_o, are therefore required to determine crack instability for flaws growing around large pores.[19]

This study is designed to extend the micromechanical description of failure from pores, which was developed to rationalize the fracture strength of ceramics as a function of grain size[6,7] to encompass fracture strength as a function of density. It complements prior studies on fracture of alumina as a function of porosity,[1–3] since a small volume fraction of artificial, spherical pores is now distributed in a porous alumina specimen. The evolution of these large, artificial pores during densification is measured directly and the fracture origin is determined in every single specimen. Evolution of pore sizes and crack tip toughness as a function of density is then combined with a computation of the stress intensity factor of semicircular cracks around spherical pores to obtain the condition of crack instability.

2. Experimental procedure

A very fine, high purity Al_2O_3 powder (Taimai DAR, Taimei Chemicals, Tokyo, Japan) was used for the bulk of this investigation. Billets for mechanical test specimens were slip cast from an electrostatically dispersed suspension (pH 3.7, 40 vol.% solids) with 2 wt.% Carbowax™ 8000 binder. In order to produce samples with artificial flaws, very low volume fractions (0.1 vol.%) of uniform polystyrene spheres [nominal radii of 25, 50, 80 and 120 μm ±1% (Duke Scientific Corporation, Palo Alto, CA)] were introduced into the suspension (the spheres burn out during subsequent heat treatment leaving behind well defined spherical pores). After mixing and ultrasonication the suspension was coagulated by the addition of NH_4Cl[20] to minimize the segregation of spheres due to buoyant forces. After casting and drying, green density was measured geometrically and the billets sintered at 1050–1350°C for 0.5 h to produce samples with relative densities varying between 0.60 and 0.99. A smaller, comparative study was performed with a coarser powder (CT 2000, Alcoa Chemie GmbH, Ludwigshafen) where fracture strength was measured at three densities lying between 63 and 85% with samples both manufactured with and without artificial pores of a starting radius of 50 μm.

Six to 10 mechanical test specimens ($25\times3\times4$ mm^3) were cut from the sintered billets, and then ground, chamfered and polished by standard diamond finishing techniques (final size of diamond grains = 1 μm). After final polishing, density was determined by the Archimedes method. Grain growth was measured by quantitative microscopy on sintered samples. At low densities it was not possible to polish and thermally etch surfaces suitable for grain size measurement, therefore grain size was estimated from fracture surfaces. The elastic modulus was measured using a sonic resonance technique, according to ASTM C 1198. Fracture strength was measured in fully articulated, four-point bending. After failure, the fracture surfaces were examined by stereo and scanning electron microscopy for failure origin, defect type, defect size and position relative to the tensile surface.

3. Results

The relative green densities achieved were 60% using the Taimei powder and 55% using the CT2000 powder. Typical microstructures at 0.60 and 0.995 relative density for samples made from Taimei powder are shown in Fig. 1. From this figure it is evident that a very high density material with small, uniform equiaxed grain size can be produced at low sintering temperatures (1350°C). The measured grain sizes increase from 0.25 to 0.60 μm during densification and are provided in Table 1.

During sintering, the polymer spheres burned out leaving spherical pores. Fig. 2 shows the measured size of the artificial defect as a function of density for four starting pore sizes. The theoretical predictions are included as full lines and derived in the discussion section.

Young's modulus as a function of density is shown in Fig. 3, including a fit for a slightly modified Phani equation.[15] During initial stage sintering Young's modulus increases without significant densification.[16] Since the Phani equation neglects this initial, steep increase of Young's modulus from zero to 40 GPa (Fig. 3), porosity, *P*, was not normalized to green density, but to a second fitting parameter, P_1. P_1 was found to be 45%, only slightly higher than the measured value for porosity of the green body of 40% for the Taimei powder. The exponent *n* was fitted to be 1.15. In Eq. (1), $E(P)$ is the porosity dependent modulus and E_{100} is the modulus for a fully dense sample (400 MPa).

$$E(P) = E_{100}\left(1 - \frac{P}{P_1}\right)^n \tag{1}$$

Fig. 4 shows the fracture strength as a function of density for all the specimens with and without artificial flaws. Theoretical predictions are also shown and are detailed in Section 4. The average strength of fully dense specimens without artificial defects was over 550 MPa. When the strength limiting flaw was an artificial defect

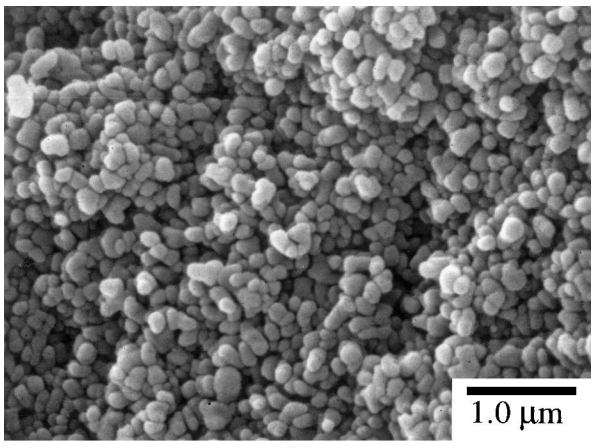

(a)

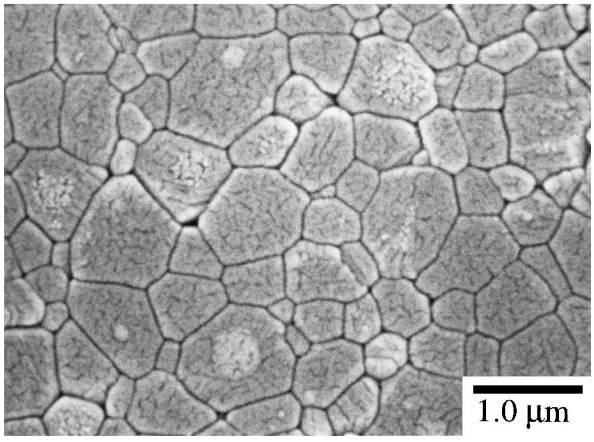

(b)

Fig. 1. Comparison of alumina microstructures for two different densities ρ: (a) $\rho = 60\%$; (b) $\rho = 99.5\%$.

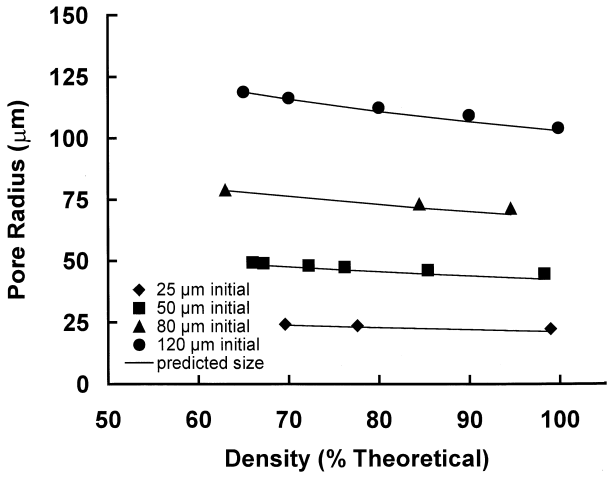

Fig. 2. Shrinkage of large, artificial pores as a function of density for $R_o = 25$, 50, 80 and 120 μm.

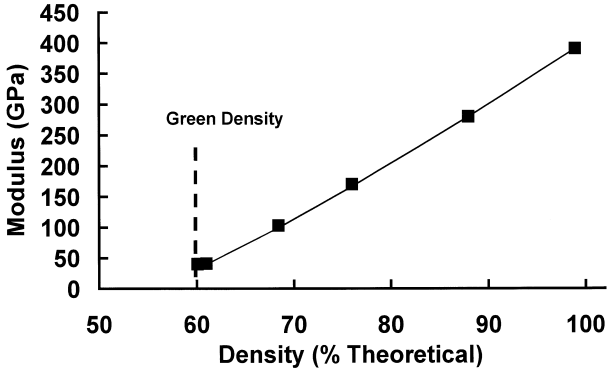

Fig. 3. Evolution of Young's modulus with increase in density, also included is full line according to Eq. (1).

Table 1
Grain size as a function of density for samples made from Taimai powder

Density (% Theo.)	63	72	76	85	99
Grain size in μm	0.25	0.26	0.32	0.38	0.60

positioned below the tensile surface (volume defect), the failure stress was corrected to reflect the stress experienced by the defect by scaling with the distance from the neutral axis. Not all specimens containing artificial pores failed from these, some also failed from natural defects. This again was dependent on size of pores and is detailed in Table 2. While 15, 22 and six data points are available for fracture from pore sizes of 25, 50 and 80 μm, only one data point (520 MPa at 99.8%) is available for pore size of 120 μm. The latter samples were difficult to produce due to cracking during drying and sintering. Fig. 4 clearly demonstrates that within statistical scatter of data, there is no noticeable effect of pore size on strength. In Fig. 4 for the data set on failure from artificial pores, only those samples that failed from a single pore are included. This point is further discussed in Section 4. Further, there is only a small difference of strength between artificial and natural defects. Finally, the more limited study on specimens prepared from a more coarse, less sinterable, but inexpensive powder yielded comparable results. In this case, the strength values were slightly below the values for the Taimei powder and the strength values for specimen with artificial defects were slightly, but consistently lower than for the specimen without artificial pores.

Fracture surface examination of modulus of rupture (MOR) samples without artificial flaws revealed that the samples predominantly failed from unidentified surface flaws, most likely polishing damage. No gross defects, such as agglomerates, or large pores, were found. Fractography of MOR specimens containing the spherical pores confirmed that the pores can act as strength limiting defects as shown in Fig. 5. The position of the strength limiting flaw was characterized with respect to the tensile surface of the test beam as a surface defect or volume defect and is included in Table 2. Fractography shows failure from artificially introduced pores with

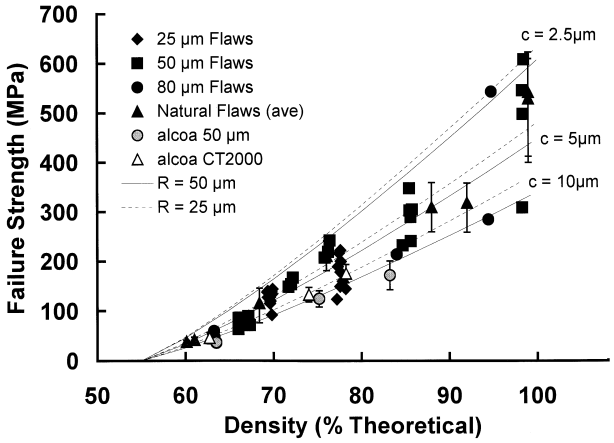

Fig. 4. Fracture strength as a function of density for artificial pores of various sizes as well as natural defects. Included are theoretical predictions of strength for specimens containing 50 μm (full line) and 25 μm (dashed line) initial pores with crack lengths, c, at instability being 2.5, 5 and 10 μm.

Table 2
Critical flaw position and frequency for various artificial pore sizes

Initial pore radius (μm)	Number of failures from artificial pores/number of specimen tested	Number of surface pores	Number of volume pores
25	15/25	0	15
50	22/50	15	7
80	6/30	4	2
120	1/20	0	1

radii from 25 to 120 μm (Fig. 5). Close examination of the fracture surrounding the artificial pores did not reveal any signs of cracking that occurred prior to or during sintering. At low densities (less than 85%) the fracture was predominantly intergranular. As density increased the fraction of transgranular fracture increased. Fracture tails were seen emanating from the bottom half of several artificial defects as shown in Fig. 6.

4. Discussion

The procedure of incorporating polymer spheres into a ceramic slip allowed production of porous specimens containing artificial crack-free pores. Fracture strengths in excess of 500 MPa are thereby achievable even with ceramics containing pores of 120 μm radius. Inclusion of polymer spheres into a ceramic slip appears to be a better technique than mixing the polymer spheres with ceramic powders and cold compacting since this may lead to cracking around the pores due to elastic spring back. It is therefore not surprising that an earlier study on Si_3N_4 containing artificial defects of 20 to 90 μm radius exhibited fracture strength values not exceeding 200 MPa.[21] The size of our pores was found to scale in a linear manner with the macroscopic shrinkage. This finding is in contrast with prior theoretical predictions where pores with size considerably larger than the grain size were predicted to grow during sintering.[9,10] It is suggested that the artificially introduced pores are of a size that their shrinkage or growth due to diffusional processes is kinetically negligible. Instead, the observed size change is related to a required compatibility of microscopic and macroscopic strain fields. Using true strains, the size of a large pore, R, at density ρ, is then related to the starting pore size, R_0, at starting density ρ_0 by Eq. (2) where V denotes the volume.

$$\int_{R_o}^{R} \frac{dR}{R} = \frac{1}{3}\int_{V_o}^{V} \frac{dV}{V} = -\frac{1}{3}\int_{\rho_o}^{\rho} \frac{d\rho}{\rho_o} \tag{2a}$$

$$\ln\frac{R}{R_o} = -\frac{1}{3}\ln\frac{\rho}{\rho_o} \tag{2b}$$

$$R = R_o\left[\left(\frac{\rho_o}{\rho}\right)^{1/3}\right] \tag{2c}$$

Eq. (2) is a slight modification to a relation suggested[13] and utilized before,[2] where engineering strain instead of true strains were considered. Shrinkage of large pores due to compatibility with the external strain field had been suggested before by Lam et al.[1] Their theoretical prediction for pore shrinkage, however, assumed that all pores disappear at the theoretical density, which in consequence lead to an extremely high strength at full density. As can be seen from Fig. 2, Eq. (2c) provides an excellent fit for the observed shrinkage of pores of all four different sizes employed.

The average properties of the material are as predicted. The elastic modulus, which should scale with the solid contact area between the grains, was well modeled by the modified Phani equation [Eq. (1)] with an exponent n of 1.15 as was used in a earlier study.[2] It should be pointed out, that Eq. (1) is merely phenomenological, but attractive for simplicity. Fundamental derivations of the contact area[22] via calculation of the equilibrium pore surface area are available for intermediate stage and final stage sintering, but lead to rather complicated numerical fits to the data. The crack tip fracture toughness, K_o, is also dependent on the contact area between sintering particles[1–3] and scales with the elastic modulus, according to

$$K_o(P) = \frac{K_{o,100}}{E_{100}}E(P) = K_{o,100}\left(1 - \frac{P}{P_1}\right)^n \tag{3}$$

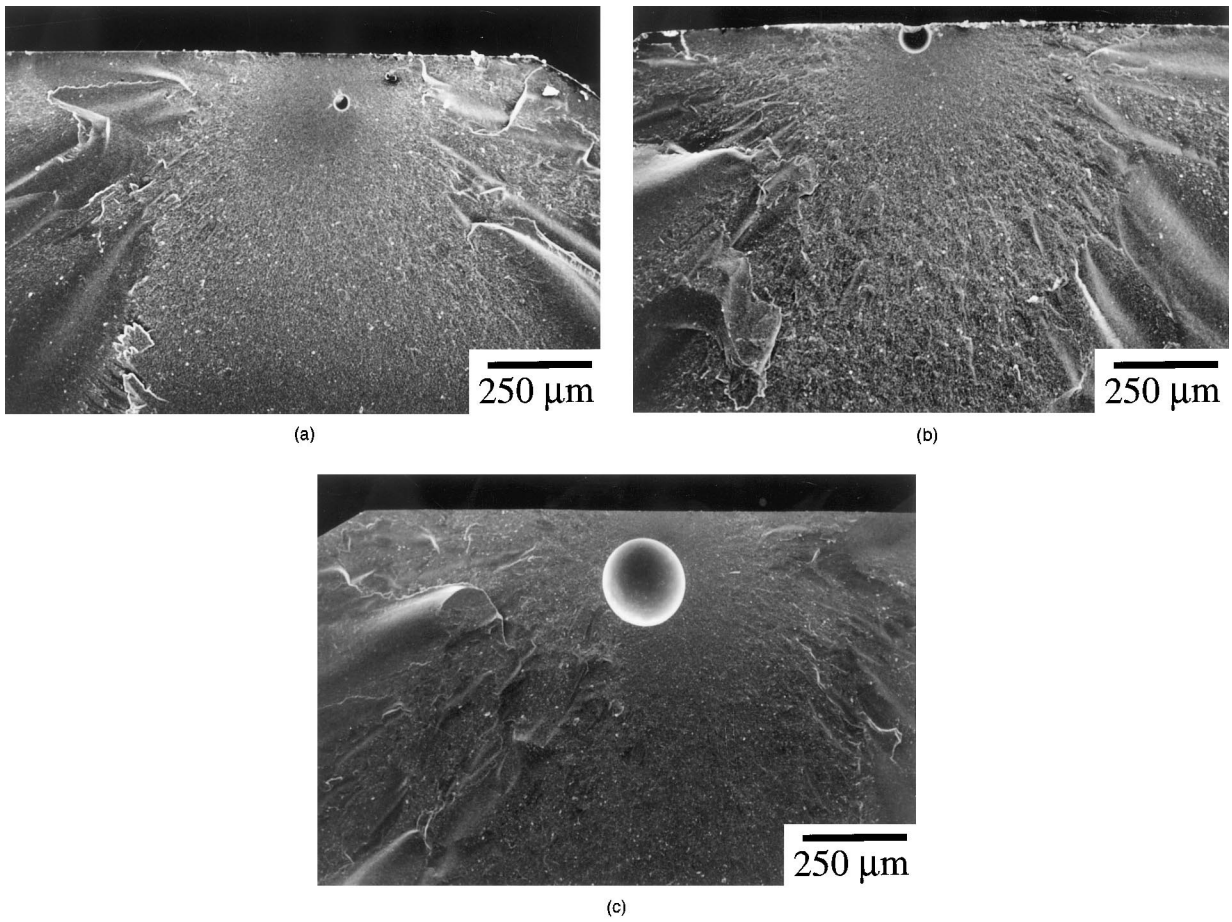

Fig. 5. Fractographic evidence that failure occurs around large artificial defects with starting pore size in green compact: (a) $R_o = 25$ μm; (b) $R_o = 50$ μm; (c) $R_o = 120$ μm. Note: fractographs are of dense samples at approximately the same magnification for comparison.

where $K_{o,100}$ is the crack tip fracture toughness of the fully dense samples. Experimental evidence for the proportionality between Young's modulus and crack tip toughness is provided in Fig. (7). The data in Fig. 7 refer to porous alumina fabricated from the Alcoa powder CT 2000. Crack tip toughness in Fig. 7 was determined from the crack opening displacement $2u(x)$ of radial cracks around Vickers indents (load = 10 kg).[23] The crack tip toughness is fitted to a parabolic crack profile according to Barenblatt[24] by a least-squares fit.

$$2u(x) = \frac{K_o}{E'}\sqrt{\frac{8x}{\pi}} \tag{4}$$

$E' = E/(1-\nu^2)$ in Eq. (4) with Poisson's ratio ν denoting the elastic modulus for plane strain. Only the crack opening displacement $2u$ for a distance $x < 60$ μm from the crack tip is used for the evaluation of the crack tip toughness. Data for densities > 75% show a close relation between Young's modulus and crack tip toughness (Fig. 7). Below 75% density, the crack system around the Vickers indents is imperfect, and the crack tip toughness data are less reliable. Previous studies have determined $K_{o,100}$ in Eq. (3) to be 2.3 $MPam^{1/2}$ on samples produced on the same powder with similar processing.[19] A contribution by crack bridging in the case of alumina where only small closure stresses pertain[17] is not required for unstable extension of cracks growing around large pores,[6,18] but only for long crack fracture toughness. SEPB fracture toughness data for porous alumina[3,23] exhibit a similar porosity dependence as provided by Eq. (3), which can be rationalized by the fact, that the number of crack bridges depends on the number of grain contacts (Fig. 7).

Failure in specimens containing artificial defects may also initiate from natural defects. This can become dominant for samples in which large artificial pores were used since the number density for large pores is reduced drastically with increasing size. The number of pores for the largest size (radius = 120 μm) drops to four for the volume in the bend bar seeing at least 50% of the maximum tensile stress (Table 3). Conversely, the number density for the smallest pore size in that volume is 458, which in some cases was observed to lead to crack initiation from a cluster of two pores with their attendant interfering stress fields. The necessity to unequivocally establish the fracture origin in every sample is therefore apparent. Data points marked as failure from

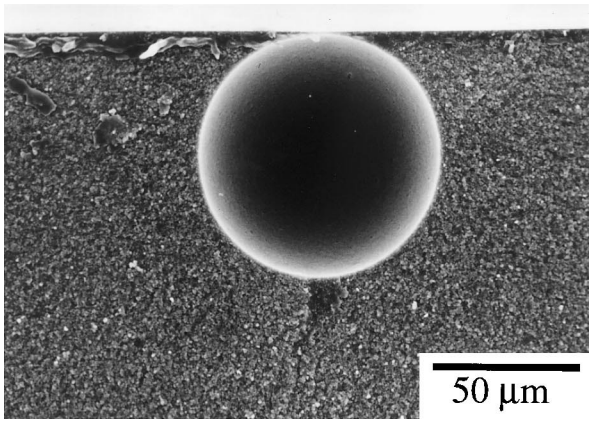

(a)

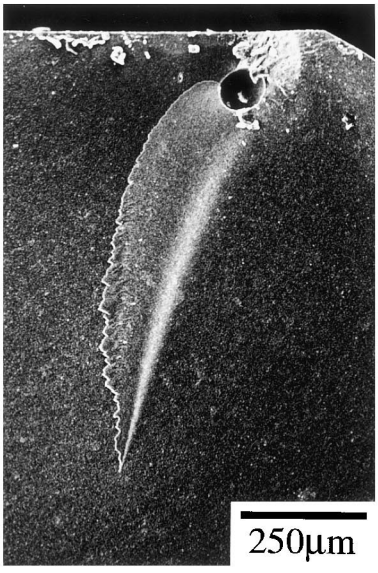

(b)

Fig. 6. Fracture tails emanating from bottom of artificial defects: (a) $R_o = 50$ μm, $\rho = 99.9\%$; (b) $R_o = 50$ μm, $\rho = 72.2\%$.

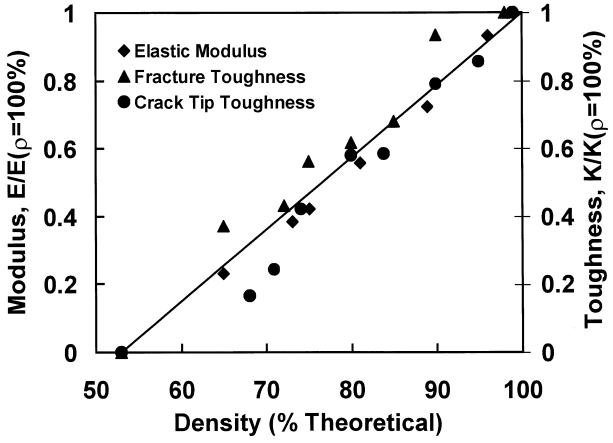

Fig. 7. Normalized Young's modulus (diamonds), crack tip toughness (circles) and SEPB fracture toughness (triangles) for porous alumina (Alcoa powder CT 2000) according to Knechtel.[23]

Table 3
Number of pores (0.1 vol.%) within highly stressed (tensile) volume

Pore radius (μm)	Number of pores
25.0	458
50.0	57
80.0	14
120.0	4

artificial pores were taken therefore only in cases where the fracture origin was identified as one single pore.

Even for well defined spherical pores with the measured fracture stress obtained at the equator of that pore, a wide distribution of fracture strength is obtained for each pore size. A large scatter of data was also obtained in a related study in Si_3N_4.[21] This may be rationalized in searching for the worst case scenario to obtain the fatal flaw in a bend specimen. Since this is a statistical effect, a large number of small pores may lead to lower strength than a small number of large pores (like in the case of a constant volume of artificial pores). The critical flaw should appear at a position where the stress field around an artificial pore is augmented by the stress field of a natural defect. This is altered by the residual stress distribution due to thermal expansion mismatch at a position where the grain sizes of the ceramic are large and the local fracture toughness is minimal. It may seem surprising, however, that the size of the largest defect has only a negligible, actually not quantifiable influence on the strength of the material. An explanation for this behavior is only afforded when more detailed fracture mechanics is considered that goes beyond equating the size of the artificial pore and the size of the failure-causing crack. We therefore note from fractographic observation (Fig. 6) and a prior study on fracture from artificial defects in dense specimens,[6] that the most likely scenario for an unstable crack configuration is one of a semicircular crack around a spherical (or semispherical) pore (Fig. 8). Therefore, the fracture mechanical treatment as outlined by Zimmermann et al.[6] is directly applicable, except that the fracture toughness and spherical pore size are density dependent. The actual procedure is only outlined here and the interested reader referred to the equations explained in detail in Ref. 6.

Assessment of the stress intensity factors is divided into two parts.[6] First, the stress distribution of the uncracked configuration is derived by means of elasticity theory. In a second step, the elastic stress distribution is integrated over the respective crack area utilizing the weight function approach. In doing so, a surface correction term for the presence of the pore surface has to be included. In order to determine crack instability, the local stress intensity factor is averaged over a virtual incremental crack surface (Fig. 8), where the assump-

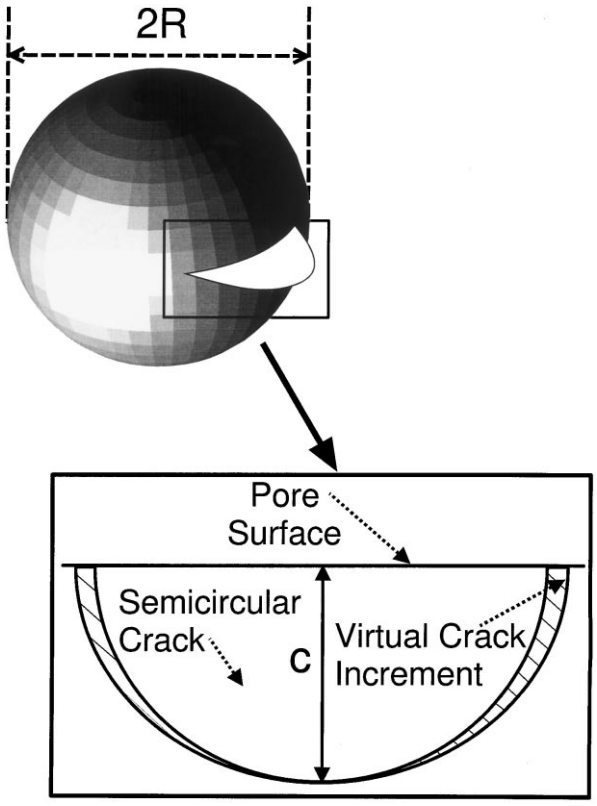

Fig. 8. Schematic depicting configuration of spherical pore with radius, R, and a semicircular crack of length, c, emanating from its surface.

tion has to be made that the semicircular crack grows predominantly along the pore surface where the tensile stresses are maximized. This leads to an averaged stress intensity factor, which at equilibrium is equal to the fracture toughness of the porous ceramic, given by Eq. (3). Depending on the actual size of the semicircular crack, which evolves upon mechanical loading, a range of fracture stresses is obtained. As the size of this semicircular crack at instability is not known a priori, the computation was performed for three different crack lengths for two different starting pore sizes, e.g. 25 and 50 μm diameter. The size of the semicircular crack, c, was assumed to be 2.5, 5, and 10 μm.

The results of our prediction for the strength of the specimen with 50 μm pore radius (full line) and 25 μm pore radius (dashed line) are included in Fig. 4. The range of fracture strength data is well covered by both envelopes provided by the assumed smallest (2.5 μm) and largest (10 μm) semicircular cracks around the artificial pore. Furthermore, the size of the artificial pore has only a small influence on the strength of the specimen. Note that the effect of pore size is less for smaller crack sizes (calculations that predict higher strength). This is rationalized by the fact that the stress concentration just outside the pore surface is independent of pore size. For specimen with small grain size, where the crack grows only a small distance away from the pore surface before it reaches instability (higher strength specimen), the stress field changes only little along the crack surface and is therefore only to a small degree influenced by pore size.[25] If the grain size is kept constant, while the pore size decreases, an increasing influence of pore size on strength is observed.[25] Nevertheless, the role of large pores can not be neglected even for alumina with a small ratio of grain size to pore size, since fracture unequivocally originates from large pores (Figs. 5 and 6). If a single theoretical prediction is sought, the crack size, c, of 5 μm around both the 25 and 50 μm pores gives the best agreement with experimental data. This crack size may be compared to the size of the semicircular crack in a dense alumina for a similar grain size[6] (0.8 μm) of 4 μm. Both crack sizes are therefore very similar. Our experimental strength data and theoretical modeling for alumina as a function of density therefore is consistent with our work on the influence of grain size on fracture strength in this material.

5. Conclusions

1. The size of the largest porous defect evolves in an almost linear fashion governed by macroscopic shrinkage.
2. The crack tip toughness scales with the elastic modulus and their density dependence is well described by established phenomenological relations.
3. Large, artificial pores serve as fracture origins in porous alumina.
4. The size of large artificial pores has only a negligible influence on the strength of ceramics provided pore size is large compared to microstructural features. This is reflected by the model, since the critical applied stress for a semicircular crack with length $c = 5$ μm decreases only by 7%, if the radius of the attached pore increases from $R = 25$ μm to $R = 50$ μm (Fig. 4).

Acknowledgements

This work was funded in part by NSF grants: DMR 9257027 and MSS 9209775.

References

1. Lam, D. C. C., Lange, F. F. and Evans, A. G., Mechanical properties of partially dense alumina produced from powder compacts. *J. Am. Ceram. Soc.*, 1994, **77**, 2113–2117.
2. Ostrowski, T., Ziegler, A., Bordia, R. K. and Rödel, J., Evolution of Young's modulus, strength and microstructure during liquid phase sintering. *J. Am. Ceram. Soc.*, 1998, **81**, 1852–1860.

3. Ostrowski, T. and Rödel, J., Evolution of mechanical properties of porous alumina during free sintering and hot pressing. *J. Am. Ceram. Soc.*, 1999, **82**, 3080–3086.
4. Baratta, F. I., Refinement of stress intensity factor estimates for a peripherally cracked spherical void and a hemispherical surface pit. *J. Am. Ceram. Soc.*, 1981, **64**, C3–C4.
5. Evans, A. G., Biswas, D. R. and Fulrath, R. M., Some effects of cavities on the fracture of ceramics: II, spherical cavities. *J. Am. Ceram. Soc.*, 1979, **62**, 101–106.
6. Zimmermann, A., Hoffman, M., Flinn, B. D., Bordia, R. K., Chuang, T.-J., Fuller, E. R. and Rödel, J., Fracture of alumina with controlled pores. *J. Am. Ceram. Soc.*, 1998, **81**, 2449–2457.
7. Zimmermann, A. and Rödel, J., Generalized Orowan–Petch plot for brittle fracture. *J. Am. Ceram. Soc.*, 1998, **81**, 2527–2532.
8. Rice, R. W., Pores as fracture origins in ceramics. *J. Mater. Sci.*, 1984, **19**, 895–914.
9. Kingery, W. D. and Francois, B., Sintering of crystalline Oxides, I. interaction between grain boundaries and pores. In *Sintering and Related Phenomena*, ed. G. C. Kuczynski, N. A. Hooton and G. F. Gibbon. Gordon Breach, New York, 1967, pp. 471–498.
10. Kellett, B. J. and Lange, F. F., Experiments on pore closure during hot isostatic pressing and forging. *J. Am. Ceram. Soc.*, 1988, **71**, 7–12.
11. Oh, K.-S., Kim, D.-Y. and Cho, S.-J., Shrinkage of large isolated pores during hot isostatic pressing of presintered alumina ceramics. *J. Am. Ceram. Soc.*, 1995, **78**, 2537–2540.
12. Evans, A. G. and Hsueh, C. H., Behavior of large pores during sintering and hot pressing. *J. Am. Ceram. Soc.*, 1986, **69**, 444–448.
13. Flinn, B. D., Bordia, R. K. and Rödel, J., Evolution of strength determining flaws during sintering. In *Sintering Technology*, ed. R. M. German, G. L. Messing and R. G. Cornwall. Marcel Dekker, New York, 1996, pp. 13–20.
14. Coble, R. L. and Kingery, W. D., Effect of porosity on physical properties of sintered alumina. *J. Am. Ceram. Soc.*, 1956, **39**, 377–385.
15. Phani, K. K. and Niyogi, S. K., Young's modulus of porous brittle solids. *J. Mater. Sci.*, 1987, **22**, 257–263.
16. Green, D. J., Nader, C. and Brezny, R., The elastic behavior of partially-sintered alumina. In *Sintering of Advanced Ceramics*. Ceramics Transactions Vol. 7. The American Ceramic Society, Westerville,1990, pp. 345-36.
17. Fett, T., Munz, D., Seidel, J., Stech, M. and Rödel, J., Correlation between long and short crack R-curves in alumina using the crack opening displacement and fracture mechanical weight function approach. *J. Am. Ceram. Soc.*, 1996, **79**, 1189–1196.
18. Seidel, J., Claussen, N. and Rödel, J., Reliability of alumina ceramics: I, effect of grain size. *J. Eur. Ceram. Soc.*, 1995, **15**, 395–404.
19. Seidel, J. and Rödel, J., Measurement of crack tip toughness in alumina as a function of grain size. *J. Am. Ceram. Soc.*, 1997, **80**, 433–438.
20. Velamakanni, B. V., Lange, F. F., Zok, F. W. and Pearson, D. S., Influence of interparticle forces on the rheological behavior of pressure-consolidated alumina particle slurries. *J. Am. Ceram. Soc.*, 1994, **77**, 216–220.
21. Heinrich, J. and Munz, D., Strength of reaction-bonded silicon nitride with artificial pores. *Bull. Am. Ceram. Soc.*, 1980, **59**, 1221–1222.
22. Svoboda, J., Riedel, H. and Zipse, H., Equilibrium pore surfaces, sintering stresses and constitutive equations for the intermediate and late stages of sintering — I. computation of equilibrium surfaces. *Acta Metall. Mater.*, 1994, **42**, 435–443.
23. Knechtel, M., Präparation und Charakterisierung metallverstärkter Keramiken mit interpenetrierenden Netzwerken. Dissertation, University of Technology, Hamburg-Harburg, 1996.
24. Barenblatt, G. I., The mathematical theory of equilibrium cracks in brittle fracture. *Adv. Appl. Mech*, 1962, **7**, 55–127.
25. Zimmermann, A. and Rödel, J., Fracture statistics based on pore/grain-size interaction. *J. Am. Ceram. Soc.*, 1999, **82**, 2279–2281.